MEASUREMENT OF WATER VELOCITY BY OPTICAL METHODS

by

GEORGE WEIMING FANG
LT USN

Course 13A May 31, 1968

MEASUREMENT OF WATER VELOCITY BY OPTICAL METHODS IN THE MIT PROPELLER TUNNEL

by

GEORGE WEIMING FANG
LT USN

S.B., University of Louisville
(1960)

SUBMITTED IN PARTIAL FULFILLMENT OF THE
REQUIREMENTS FOR THE DEGREE OF
NAVAL ENGINEER
AND
MASTER OF SCIENCE IN ELECTRICAL ENGINEERING

at the

MASSACHUSETTS INSTITUTE OF TECHNOLOGY

June, 1968

MEASUREMENT OF WATER VELOCITY BY OPTICAL METHODS

IN THE MIT PROPELLER TUNNEL

by

GEORGE WEIMING FANG
LT USN

Submitted to the Department of Naval Architecture and Marine Engineering and the Department of Electrical Engineering on May 31, 1968, in partial fulfillment of the requirements for the degrees of Naval Engineer and of Master of Science in Electrical Engineering.

ABSTRACT

An optical system to detect and measure the flow velocity in the MIT propeller tunnel was built, based on the theory proposed by M.J. Block and J.H. Milgram in a paper to the Optical Society of America. The method involved the detection of reflected light radiation off air bubbles in the water. This radiation, after being spatially filtered by a reticle, is collected by a photomultiplier and temporally filtered by a bandpass filter. The frequency of the resultant signal is a function of the flow velocity.

Results of the investigation show a general agreement to within 3% between the velocities obtained by this method and that obtained by means of the pitot-static tube. Difficulties encountered in the investigation are enumerated, and recommendations are made for possible future investigations.

Thesis Supervisor: Jerome H. Milgram
Title: Assistant Professor of Naval Architecture

Acknowledgement

I wish to thank Professor J.H. Milgram whose theories on optical detection of flow velocity were behind the investigation, and whose translation of the mathematics of statistical optics into everyday terms were necessary to this investigation.

I also wish to thank Mr. Robert Ashworth, of the MIT propeller tunnel, who has been most valuable in instructing me in the use of the shop in his care. My special thanks go to Mr. Lawrence Ting, of the Polaroid Corp., who managed to procure the various photodetectors tried including the photomultiplier finally used.

Table Of Contents

Table of Figures

1. Introduction

The purpose of this paper is to report on the investigations conducted towards the detection of local flow velocity, by optical means, in the MIT propeller tunnel. The theory behind the method of detection is entirely based on that set forth by M.J. Block and J.H. Milgram (1) who proposed that spatial and temporal filtering of optical radiation observed from a position outside a flow will enable one to detect the local fluid flow velocity.

Flow velocity measurement, in current engineering practice, is concerned primarily with measurement of surrogate properties such as dynamic pressure. We present in the following a brief survey of the instruments and/or methods presently popular, with comments.

a. Pitot tube. The most commonly employed instrument here is the Prandtl-type pitot-static tube, a device which, accompanied by a manometer, will indicate the difference between dynamic pressure and static pressure. Velocity of the flow is obtained by $V=C\sqrt{2g\gamma\Delta h}$, where γ is the density ratio between the densities of the manometer fluid and of the flow. For the Prandtl-type pitot-static tube, C=1 gives excellent results. Furthermore, this instrument is relatively insensitive to orientation with the direction of flow, up to about 15 degrees misalignment. A disadvantage

is, of course, that it is a disturbing type of measurement since the instrument must be introduced into the stream of interest. A further disadvantage is the fact that it is slow to respond to fluctuations in velocity. To improve accuracy with greater misalignment than 15 degrees, a Kiel probe may be used which can measure stagnation pressures to within 1% accuracy up to $\pm$54 degrees misalignment (3), with the accompanying disadvantage of requirement for a separate instrument to measure static pressure.

b. Current Meter. Whether the current meter be composed of vanes or cups, rotating about an axis normal or parallel to the flow, this type of measurement again disturbs the flow, to a greater extent than the pitot tube.

c. Hot-wire. The hot-wire, generally made of platinum or tungsten on the order of thousandths of an inch depends on the fact that its resistance is a function of temperature which in turn is dependent on the heat lost to the surrounding fluid. The coefficient of heat transfer increases with increasing velocity of the fluid. Although this method can measure local velocity at a point and is sensitive to velocity fluctuations, the disadvantage is fragility

of the wire in high fluid density and velocity and the existence of possible non-linearity.

d. Bulk or average measurements. The methods for determination of bulk flow velocities or average velocities over a cross section are not of interest here, since these are unable to detect velocities at a point. Among such methods can be listed the venturi meter; orifice meter; electromagnetic, thermal, or ultrasonic flow meters.

e. Optical methods. The present uses of optics in fluid velocity detection are primarily concerned with photographic effects. For compressible fluids there exist the Schliern apparatus, the shadowgraph, and the Mach-Zender interferometer (9). For measurement of local velocities in water, one photographic method is to inject small spheres of a mixture of benzene and carbon tetrachloride and to photograph them. The measurement of the distance travelled by these bubbles, of the same specific gravity as water, between timed successive exposures will give a determination of the water velocity (3). A refinement of the above method has been accomplished by Stewart (10) who injected "micro bubbles" of a plastic material into a stream and, triggering photomultipliers by the light reflected off these spheres, measured the

transit time between a fixed distance.

The last method just described leads into the area investigated for this report, the detection of local fluid flow velocities by optical means. Specifically, the investigation involved the construction of an optical system to detect the flow velocity of water in the variable pressure propeller tunnel maintained by the Department of Naval Architecture and Marine Engineering.

2. Theory

The theory of image formation, object space isolation and temporal and spatial filtering of radiant energy reflected off randomly spaced bubbles moving with a fluid flow is that set forth by Block and Milgram (1).

The assumptions in this problem are the following:

a. The flow is one-dimensional, i.e., the velocity vector is directed only along the propeller tunnel's longitudinal axis.

b. The flow is uniform and constant over the period of observation.

c. The process which generates the illumination, i.e. the light reflected off randomly distributed moving bubbles, is stationary, so that averages can be taken over time, space or both.

A diagram of the situation is presented below.

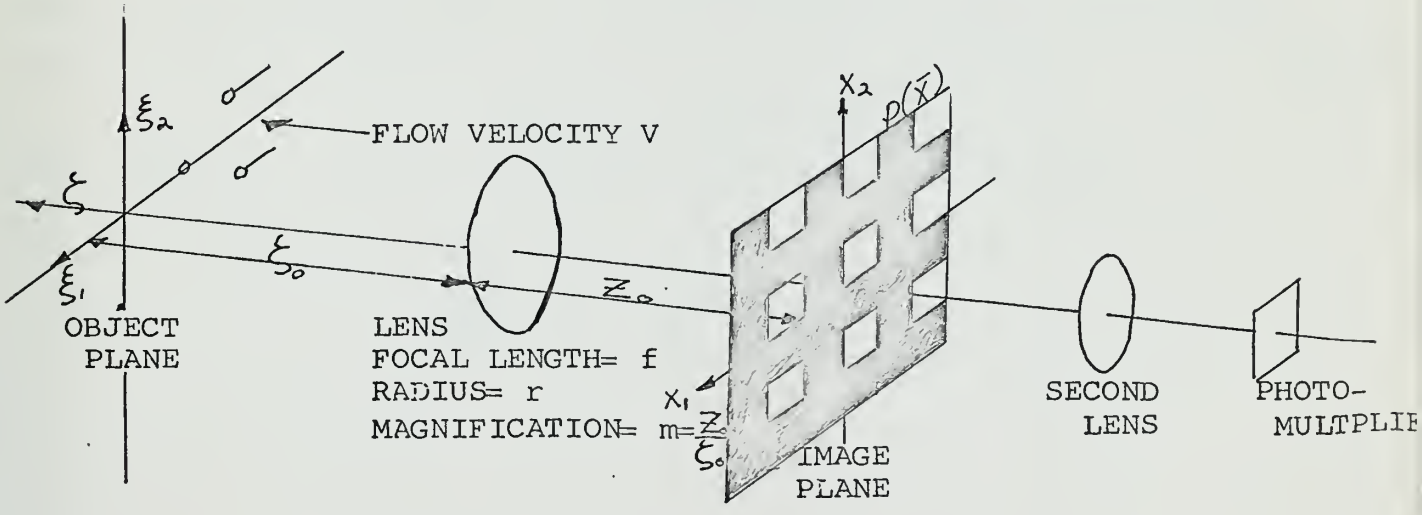

FIG 1

Let $\ell(\bar{\xi}, \xi, t)$ = the rate of reflected radiant energy per unit volume per unit time at a time t.

$s(\bar{x}-m\bar{\xi}, \xi)$ = the spread function, or the illumination produced by a point source of unit intensity on the object plane.

$i(\bar{x}, t)$ = the illumination of the image plane.

Define $dA\bar{x} = dx_1 dx_2$, and integrals of the form $\lim_{B\to\infty} \int_{-B}^{B}$ will be written without limits.

$i(\bar{x},t)$ is a convolution of $\ell(\bar{\xi}, \xi, t)$ and $s(\bar{x}-m\bar{\xi}, \xi)$, such that

$$i(\bar{x}, t) = \iiint \ell(\bar{\xi}, \xi, t)\, s(\bar{x}-m\bar{\xi}, \xi)\, dA\bar{\xi}\, d\xi$$

Now $$s(\bar{x}-m\bar{\xi}, \xi) = \mathcal{R}^2/4\pi\xi_0^2 c^2 \xi^2 \qquad |\bar{x}-m\bar{\xi}|^2 \le (c\xi)^2$$
$$= 0 \qquad \text{elsewhere}$$

as is shown in Appendix 2, where it is assumed that $\xi \ll \xi_0$ so that a first order approximation is used, and where the derivation uses the laws of geometric optics.

The two-dimensional Fourier transform if s is

$$S(\bar{\omega}_p, \xi) = \mathcal{R}^2 J_1(\omega c \xi)/2\xi_0^2 \omega c \xi$$

Now if the intensity $i(\bar{x},t)$ is passed through a filter $p(\bar{x})$, then $p(\bar{x})$ is of the form $p_1(x_1)p_2(x_2)$, so that its transform

$$P(\bar{\omega}_p) = P_1(\omega_1)\, P_2(\omega_2)$$

See Appendix 3, for the representation of the filter used.

The autocorrelation of g(t) is

$$\phi_{gg}(\tau) = \langle g(t)\, g(t+\tau) \rangle$$

Now, $g(t) = \iint i(\bar{\alpha}, t)\, p(\bar{\alpha})\, dA_{\bar{\alpha}}$

and $g(t+\tau) = \iint i(\bar{\beta}, t+\tau)\, p(\bar{\beta})\, dA_{\bar{\beta}}$.

Therefore $\phi_{gg}(\tau) = \iiiint dA_{\bar{\alpha}}\, dA_{\bar{\beta}}\, p(\bar{\alpha}) p(\bar{\beta})\, \phi_{ii}(\bar{\alpha}-\bar{\beta}, -\tau)$.

Since the velocity is assumed to be uniform,

$$\phi_{ii}(\bar{\alpha}-\bar{\beta}, -\tau) = \phi_{ii}(\bar{\alpha}-\bar{\beta}-m\bar{v}\tau, 0)$$

By inverse transformation,

$$\phi_{ii}(\bar{\alpha}-\bar{\beta}-m\bar{v}\tau, 0) = \frac{1}{4\pi^2} \iint \Phi_{ii}(\bar{\omega}_p, 0) \exp -i(\bar{\alpha}-\bar{\beta}-m\bar{v}\tau)\cdot\bar{\omega}_p\, dA_{\bar{\omega}_p}$$

and

$$\phi_{gg}(\tau) = \iiiiiii \frac{1}{4\pi^2} p(\bar{\alpha}) e^{+i\bar{\alpha}\cdot\bar{\omega}_p} dA_{\bar{\alpha}}\, p(\bar{\beta}) e^{-i\bar{\beta}\cdot\bar{\omega}_p} dA_{\bar{\beta}}\, e^{-im\bar{v}\tau\cdot\bar{\omega}_p} \Phi_{ii}(\bar{\omega}_p, 0)\, dA_{\bar{\omega}_p} \qquad (a)$$

There now only remains a consideration of $\Phi_{ii}(\bar{\omega}_p, 0)$.

As demonstrated by Block and Milgram,

$$\Phi_{ii}(\bar{\omega}_p, 0) = m^2 \iint \Phi_{ee}(m\bar{\omega}_p, \xi_2-\xi_1, 0)\, S(-\bar{\omega}_p, \xi_1)\, S(\bar{\omega}_p, \xi_2)\, d\xi_1\, d\xi_2 \qquad (b)$$

This is derivable from a consideration of the spatial autocorrelation of $i(\bar{x}, t)$. By decomposing $\Phi_{pp}(\bar{u}, \ldots)$ into $\Phi_{p1}(\bar{u}, \ldots, u_o) + \Phi_{p2}(\bar{u}, \ldots, u_o)$ the authors showed that, $\Phi_{iK}(\bar{\omega}_p, 0, \omega_o) = m^2 \iint \Phi_{eK}(m\bar{\omega}_p, \xi_2-\xi_1, 0, m\omega_o) S(-\bar{\omega}_p, \xi_1) S(\bar{\omega}_p, \xi_2)\, d\xi_1\, d\xi$

where $\Phi_{p1}(\bar{u}, \ldots, u_o) = \Phi_{pp}(\bar{u}, \ldots) \quad |\bar{u}| < u_o \qquad K = 1, 2 \qquad (c)$

$= 0 \quad |\bar{u}| \geq u_o$

and similarly, $\Phi_{p2}(\bar{u}, \ldots, u_o) = 0 \quad |\bar{u}| < u_o$

$= \Phi_{pp}(\bar{u}, \ldots) \quad |\bar{u}| \geq u_o$

Φ_{i1} contains no signals of interest, since it is zero for $|\bar{\omega}_p| \geq \omega_o$ and, with image motion due to flow velocity, the radian frequency $m\omega_o V$ is contained in Φ_{i2}. Therefore, high pass filtering of Φ_{ii} can eliminate the effect of Φ_{i1}.

The ξ directed isolation in Φ_{i2} is of interest. Returning to equation (c) for k=2, one can consider Φ_{e2} to be weighted by $S(-\bar{\omega}_p, \xi_1) S(\bar{\omega}_p, \xi_2)$ in the integral. Since, $S(\bar{\omega}_p, \xi) = \frac{r^2}{2\xi_0^2} \frac{J_1(\omega_c \xi)}{\omega_c \xi}$

$$\int_0^\infty d\xi \, S(\bar{\omega}_p, \xi) = \frac{r^2}{2\xi_0^2} \frac{1}{\omega_c}$$

and expansion of $J_1(\omega_c \xi)$ into an asymptotic expression for large $\omega_c \xi$ shows that $\int_0^\infty d\xi \, |S(\bar{\omega}_p, \xi)| < \frac{r^2}{2\xi_0^2 \omega_c} \left(\frac{2}{\pi}\right)^{1/3} \frac{1}{(\omega_c B)^{3/2}}$

if A is the ratio of the weight given to the integral over a length $2\xi_e$, centered about $\xi = 0$, to the weight given to the integrated absolute value outside of this interval, then

$$A > \left(1 - \frac{2}{\pi(\omega_c \xi_e)^3}\right) \Big/ \left(\frac{2}{\pi(\omega_c \xi_e)^3}\right)$$

This expression will be of interest in the Results and Conclusions section. In any case, if A is large enough,

$$\Phi_{i2}(\bar{\omega}_p, 0, \omega_0) = \Phi_{e2}(m\bar{\omega}_p, 0, 0, m\omega_0) \, m^2 r^4 / 4\xi_0^4 \omega^2 c^2 + \text{small error}$$

Returning to equation (a), one can say that $\phi_{gg}(\tau)$ contains terms with frequencies below $\frac{\omega_0 m |\bar{v}|}{2\pi \tau}$, which can be high pass filtered out, and g(t) contains frequencies in bands centered at $\frac{m}{2\pi}(\omega_1 v_1 + \omega_2 v_2)$ and harmonics thereof. Since in this investigation, we align the reticle so that $v_2 = 0$, $f = \frac{m v_1}{\lambda}$ where λ is the reticle wavelength. The harmonics may be filtered out by a bandpass filter, as well as the frequencies below $\frac{m v}{\lambda}$. The frequency passed is a direct indication of flow velocity.

3. Description of the Investigation

The MIT variable pressure propeller tunnel test section is of a square cross-section, 20 inches by 20 inches internal dimensions, surrounded by windows of plexiglass 2 inches thick (index of refraction 1.49). The velocity of the flow is controllable by varying the RPM of an impeller. Velocities as high as 30 fps can be reached, the flow being everywhere parallel to the windows. During operations with the tunnel at atmospheric pressure, there exist many fine bubbles of air, assumed to be at the velocity of the water after steady state conditions are reached.

Investigation of these bubbles by means of photographs showed that they are spaced, on the average, 0.3 cms apart. This mean separation does not change appreciably with vertical distance except at the walls of the tunnel.

The optical system constructed consisted primarily of a condenser lense of 9 inches focal length and 6.5 inches diameter, resulting in an r/f of 0.36. The lens was mounted on one end of an aluminum tube of 0.25 inch wall thickness. The image plane is a circular 0.25 inch thick plate closing off the tube. A 2.25 inch square aperture was cut in the plate , over which was mounted a piece of ground glass. The reticle was then superimposed on the ground glass.

The reticles were made from Polaroid type 146L high-contrast line projection film. It was hoped that some forms of accurate reticle would be available commercially. However, the mean

bubble separation existent dictated a coarser lines/cm than was readily available. The method used to make these reticles was as follows. A master black and white grid network was first laid out, using Dymo plastic labelling tape of 0.25 inch width. Photographs of the master were then taken with a Polaroid model 110B camera on a Polaroid model 208 copy stand. A series of reticles were made at different magnifications. The reticles used were four in number. Their space frequencies are given in Appendix 3.

Many photodetectors were tried, ranging from solar cells to CdS cells to photodiodes integrated with a Darlington pair amplifier to a photo-FET. The detector used was a 931A photomultiplier with approximately 90 volts per dynode. To project the reticle area onto the photocathode area, a 50 mm, f/2, Schneider-Kreuznach camera lens was used.

The electronic system is composed of the following. The output of the photomultiplier is connected to a frequency analyzer, with an internal gain of 40 db and a bandpass filter variable from 6% of the center frequency to 29%, at the half power points. The center frequency is tunable from 20 cps to 20,000 cps. The output of the analyzer is connected to both an oscilloscope and an electronic counter.

The lighting system used was a 500 watt slide projector with the lamp connected to 125 volts, three phase rectified DC source. The ripple voltage was measured at less than 5 volts, and the photodetector output was monitored to

to be more than -100 dbs with reference to 1 volt. A 0.25 inch slit was inserted into the slide carrier, resulting in a plane sheet 0.50 inch in depth in the object space.

The lens system, after mechanical alignment, was mounted on a vertical post, enabling the lense barrel to scan the vertical distance of the tunnel, and the lens barrel could move in a longitudinal direction to focus on planes normal to the transverse distance of the tunnel. Alignment of the axis of the lens barrel to the normal to the window was accomplished visually by means of the reflected image in the plexiglass.

The procedure followed was as follows:

1) Illuminate the tunnel from below

2) Start the impeller so as to obtain streams of bubbles.

3) Visually focus the lens system and align the reticle to the direction of flow.

4) Tune the bandpass filter to approximately expected frequency and search for a maximum indication on the analyzer meter.

5) Record the counts on the electronic counter for 0.1 sec and 1 sec intervals.

6) Obtain photograph of the oscilloscope trace

7) Record the pitot tube manometer reading.

The magnification of the optical system was found experimentally by immersing a ruler into the test section and focusing on it by means of the ground glass. The m value used was 1.08. This value was not observed to vary with variation of transverse distance into the tunnel.

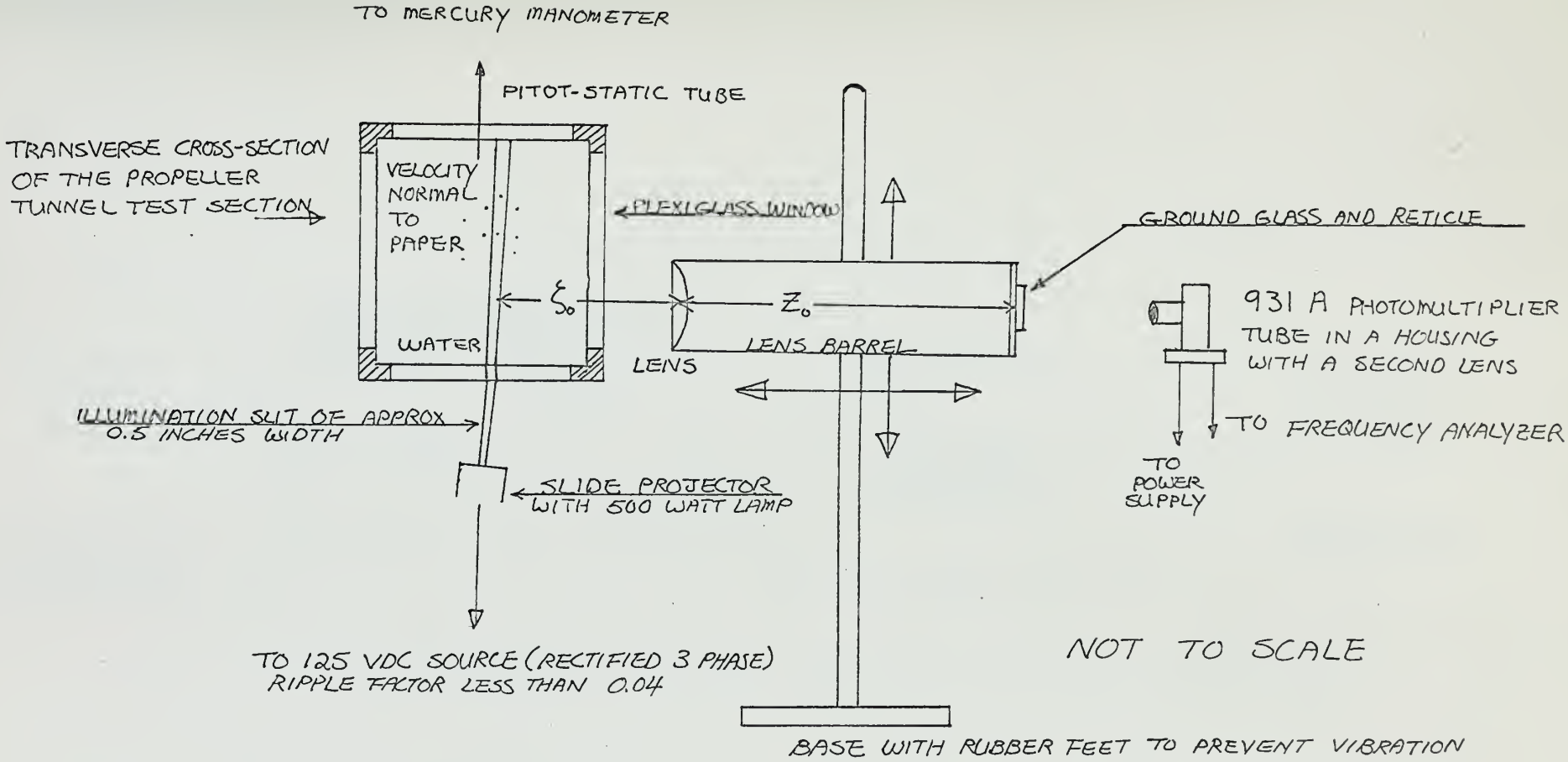

Fig 2

SCHEMATIC DIAGRAM OF EXPERIMENT

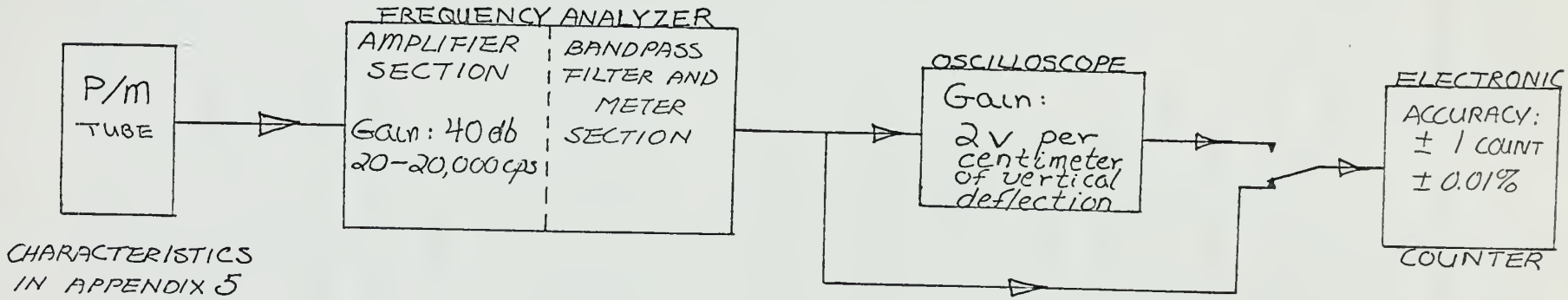

ALL INTERCONNECTIONS ARE MADE WITH RG-59/U COAXIAL CABLE

BLOCK DIAGRAM OF ELECTRONIC INSTRUMENTATION

Fig 3

4. Results and Conclusions

The experiment was conducted as outlined, with four reticle sizes used and three velocity ranges explored. Three ways of measuring the frequency were employed. The electronic counter was used to measure the frequency in a 0.1 sec interval and a 1 sec interval. Photographs of oscilloscope traces were also obtained, and the sweep speed of the trace was recorded. A third frequency was then measured from the trace.

The results are displayed in three graphs:

a. Figure 10 displays the ratio of velocity calculated from the frequency to that measured by the Pitot tube. The results for all three types of measurement are shown on the single graph. The experimental points determined by each separate reticle are joined for clarity.

b. Figure 11 is a plot of photomultiplier output as a function of m times the reticle space frequency. The parameter used was the velocity range; high, medium and low.

c. Figure 12 is a display showing that frequency is a function of velocity. Lines whose slope are exactly m/λ are drawn for reference. Data points are frequency obtained from a 0.1 sec count plotted against v_o, obtained from pitot tube measurements.

The general conclusion to be drawn is that velocities can be detected by the optical method with an accuracy of 5% or less as compared to the measurement obtained by means of a pitot tube. There is no drastic difference between the measurements from the 0.1 sec count and the 1.0 sec count. However, the spread of the data points from the photographic count is much wider than that of the first two, as would be expected.

There are some interesting trends indicated by Figure 10,

however. The consistency of the patterns formed by the reticles of various spacings leads us to suspect some biased error. Since the magnification is held constant throughout, and the alignment of the reticle with the flow is maintained for any one reticle, one suspects immediately that an error has been made in the measurement of reticle spacing. The reticles were measured with calipers and straight edge instead of on a microscope staging. However, a total error of 10% is still not likely, This discrepancy merits further attention in the future, with more accurate equipment.

Observation of the sample oscilloscope traces show that modulation is present. There is a rough correlation between the number of cycles in an envelope and the number of reticles spaces scanned: the coarser the grid, the fewer the cycles in an envelope. With reference to Appendix 3, it is obvious that N, the number of lines in the reticle, is insufficient.

Figure 11 definitely indicates that grid spacing influences the voltage output of the photomultiplier. Based on the previously observed 0.3 cm mean bubble spacing, the grid spacing of 3.33 lines/cm should have been the optimum. It is most unfortunate that no higher frequency reticles were tried in order to observe whether or not an optimum exists.

The problems presented by the measurement of water velocity in the propeller tunnel is as follows. The mean bubble separation of the bubbles being approximately 0.3 cm, a large object space needs to be scanned. However, limitations are

imposed by the distortion of magnification from angular variations. Therefore, we recommend further investigation into the effect of scanning longer distances in the object plane.

Secondly, through an unfortunate oversight in design discovered too late, much larger magnifications should have been used. As shown by Block and Milgram (1), the amount of ξ direction isolation is proportional to c to the third power, where

$$c = \frac{m^2 r}{(m+1)f}$$

$\frac{r}{f}$ as previously mentioned is 0.36 for the lens chosen. Therefore, the magnification should have been much greater than 1. Other complications entering into this problem are the limited space of the propeller tunnel room, and the desire to isolate any point in one quadrant of the test section. The first complication arises because as magnification increases, the image distance goes as (m+1). The walls of the room became practical limits if no angles in the light path are entered into. The second complication arises because, if it is desired to focus on any point from the wall of the test section to its center, a distance of ten inches, the object distance must be approximately 12 inches, taking the plexiglass into account. Since

$$\text{Object distance} = f\left(\frac{1+m}{m}\right),$$

this limits m to approximately 3. The value of m = 1 was chosen on the basis of weight of the lens barrel and ease of handling. As a result, the ξ directed isolation was not good, as evidenced by the wide spectrum of frequencies observed about the center

frequency. The isolation was maintained through the use of slit illumination of 0.5 inches depth.

We recommend for future investigations, the employment of a mirror lens, with possible f- numbers of 0.7 (5), or

$$\frac{r}{f} = 0.7$$

Also we recommend the use of as large a magnification as possible. A third avenue of exploration is the use of existing large diameter equipment mounting holes in the plexiglass, to eliminate the water - plexiglass - air interface.

A final possible future investigation is in the area of fluctuating velocity in a turbulent flow. As mentioned by Daugherty and Franzini (3), the velocity at any one point will fluctuate with time in a turbulent flow. Using a hydraulic radius of $\frac{L}{4}$, where L = 20 inches, we find that the Reynolds number is well about 2000. This possibly could account for the fluctuations in the counter readings over a period of time, and merits further investigation.

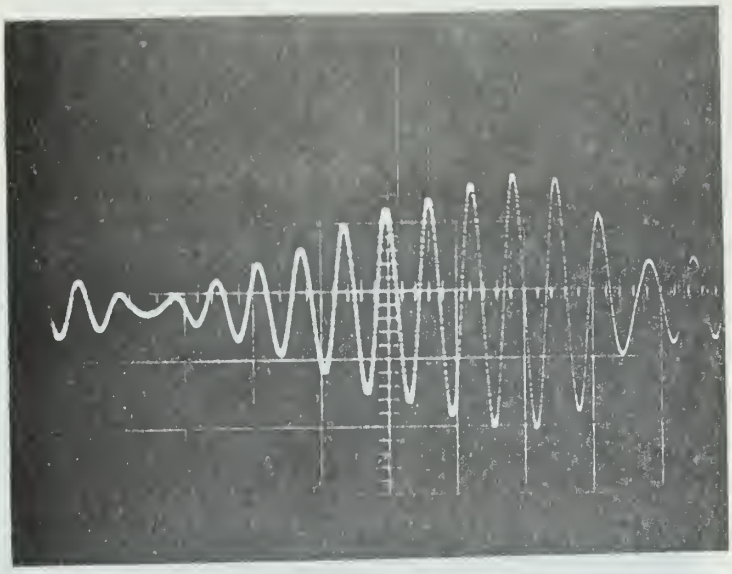

Fig. 4. Oscilloscope trace of time signal filtered through a 6% bandpass filter, grid frequency 1.67 lines/cm, temporal frequency 775 cps, velocity of flow 460 cm/sec.

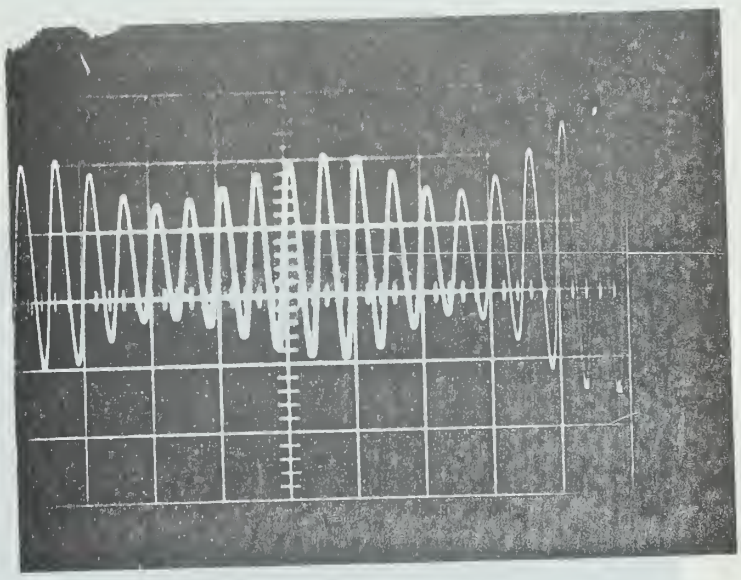

Fig. 5. Oscilloscope trace of time signal filtered through a 6% bandpass filter, grid frequency 2.29 lines/cm, temporal frequency 1980 cps, velocity of flow 800 cm/sec.

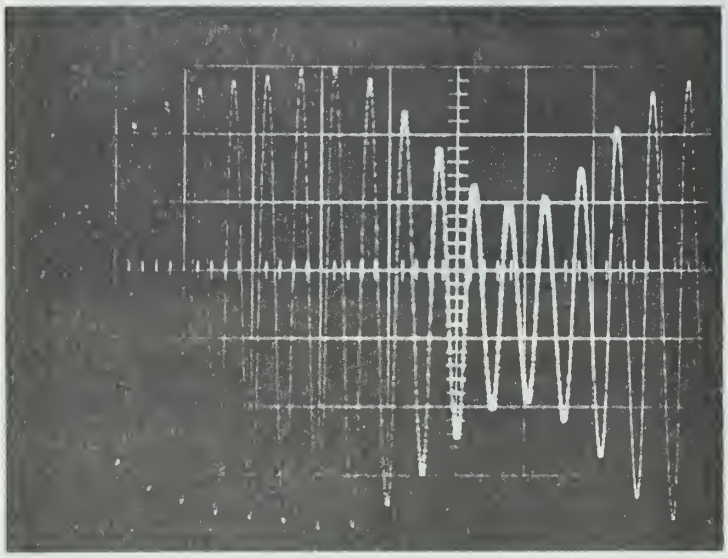

Fig. 6. Oscilloscope trace of time signal filtered through a 6% bandpass filter, grid frequency 2.92 lines/cm, temporal frequency 1935 cps, velocity of flow 620 cm/sec.

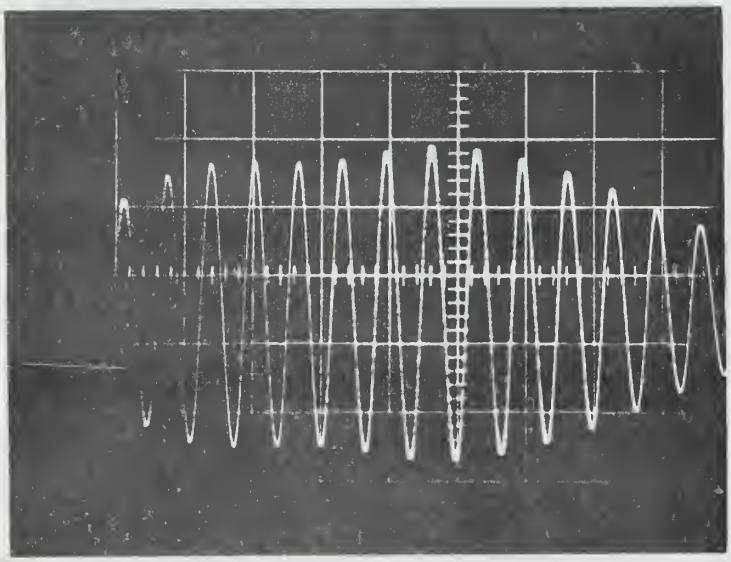

Fig. 7. Oscilloscope trace of time signal filtered through a 6% bandpass filter, grid frequency 3.33 lines/cm, temporal frequency 1530 cps, velocity of flow 425 cm/sec.

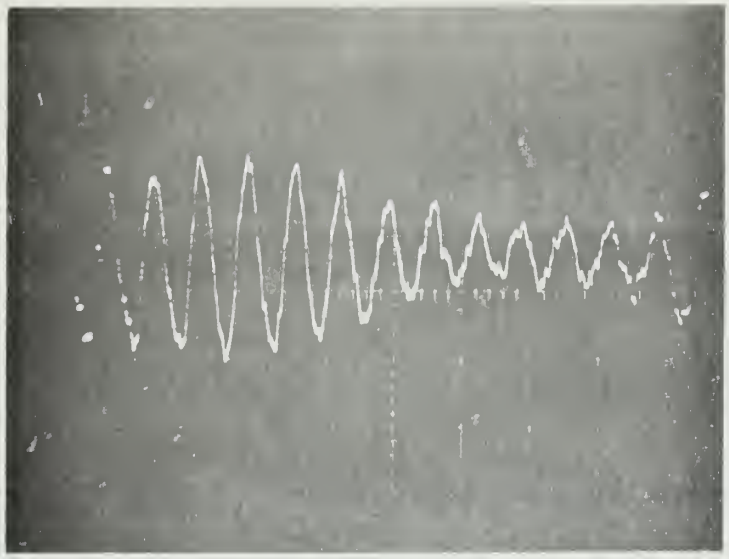

Fig. 8. Oscilloscope trace of representative signal passed through a broad band filter as described on page 13.

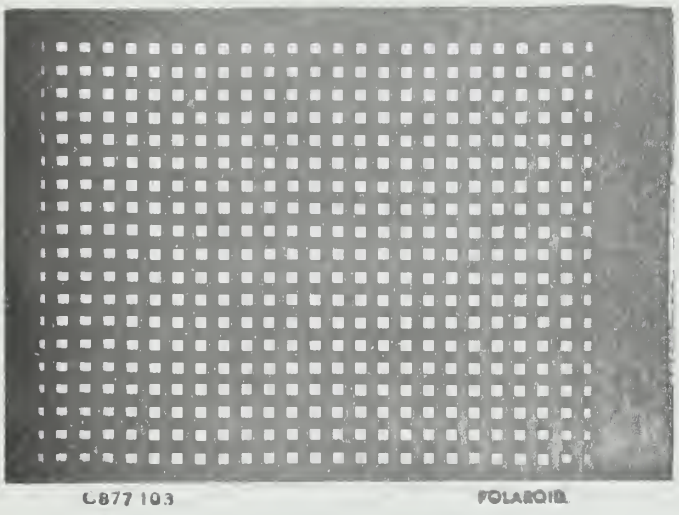

Fig. 9. Sample of reticle made on Polaroid type 146L film. The space representation and Fourier transform of this type of reticle is described in Appendix 3.

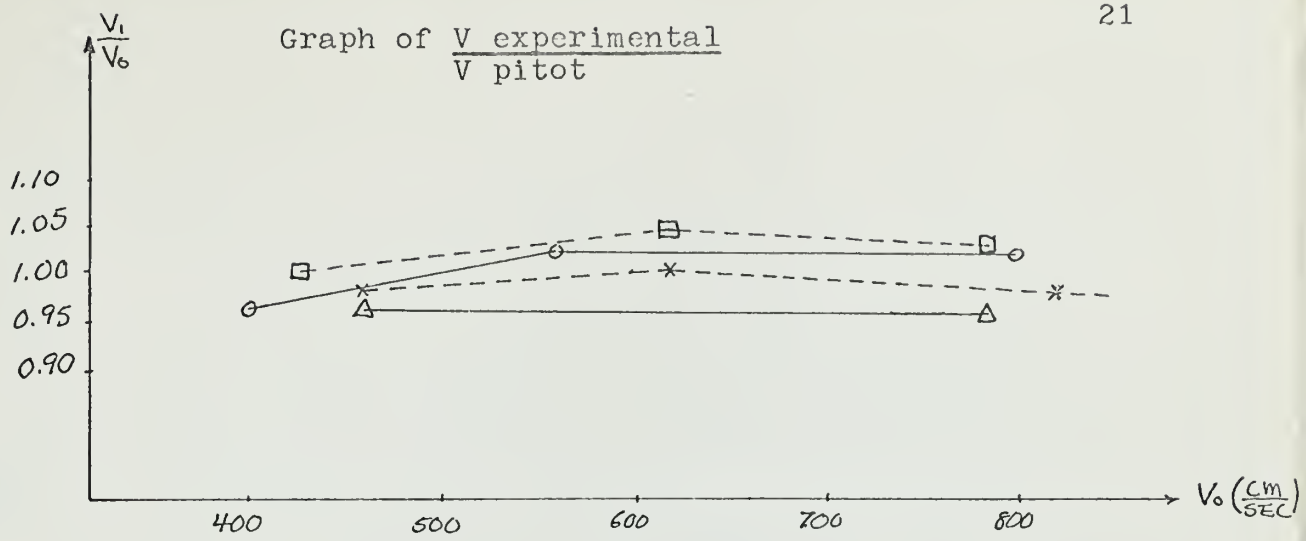

(a) V_1 based on 0.1 second count

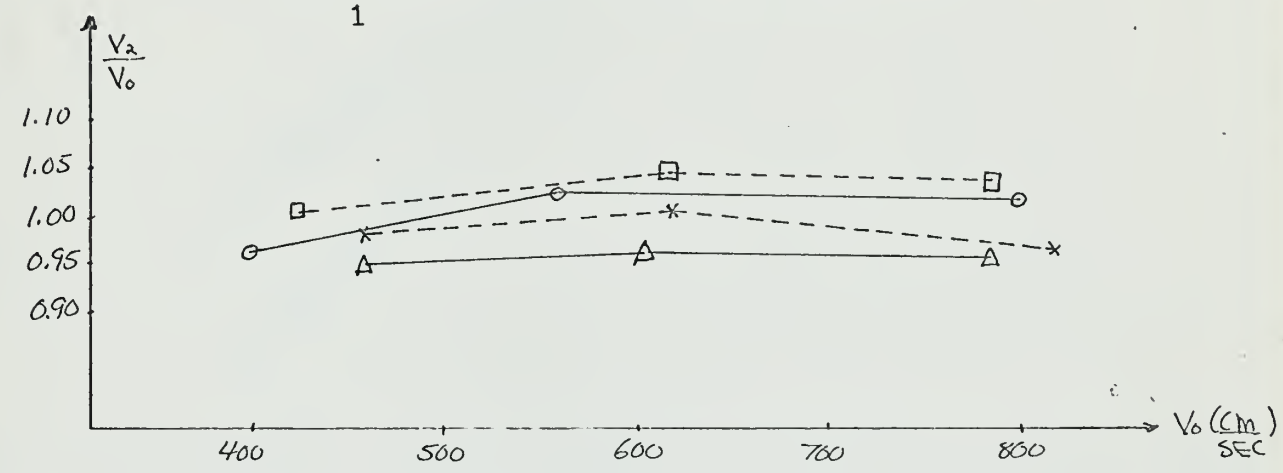

(b) V_2 based on 1.0 second count

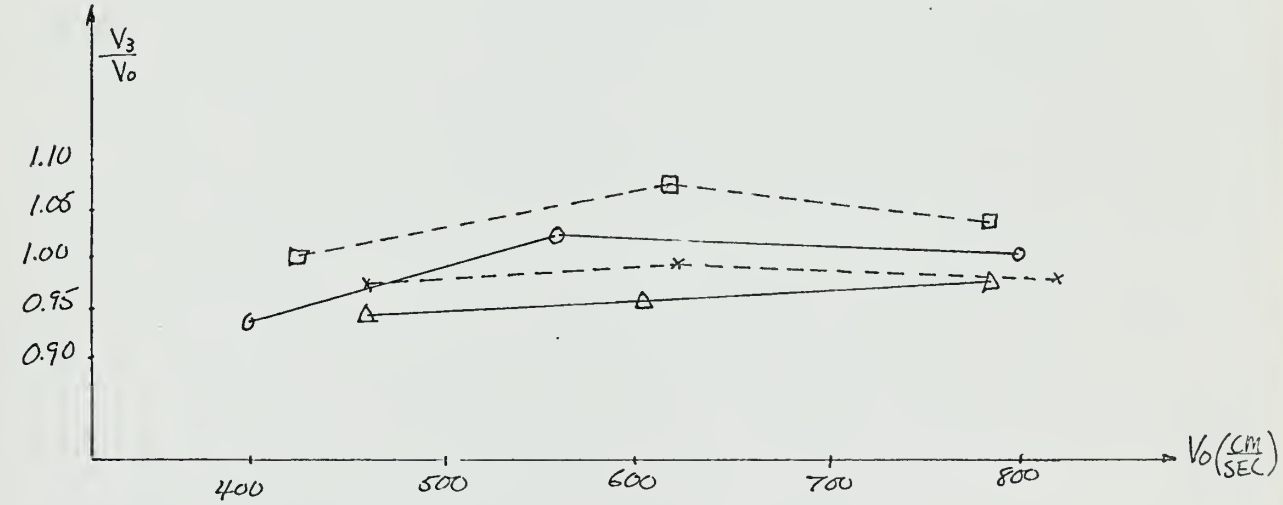

(c) V_3 based on photographic count

△ - = 1.67 lines/cm
○ - = 2.29 lines/cm
× - = 2.92 lines/cm
□ - = 3.33 lines/cm

Fig. 10

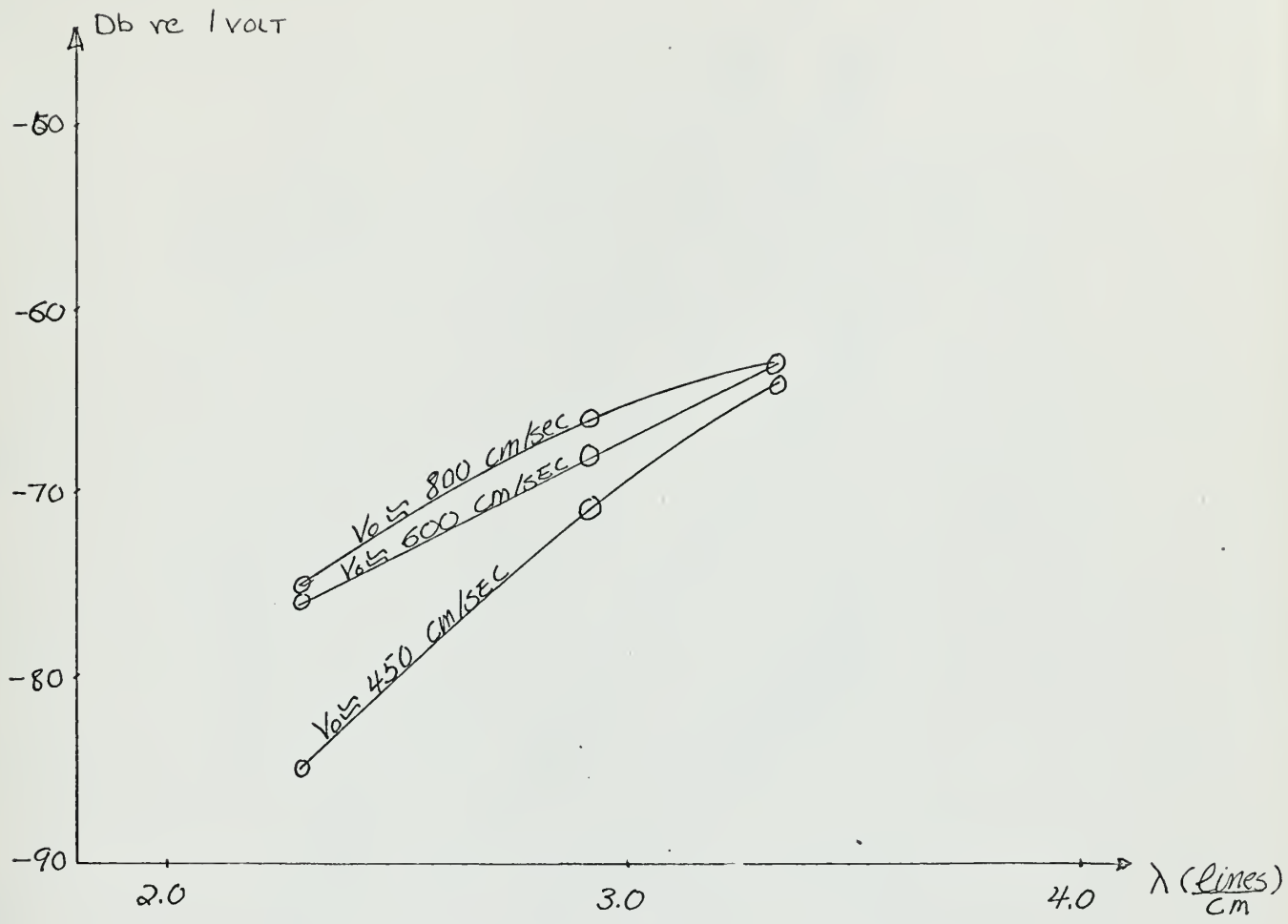

Graph of Photomultiplier Output for Various Reticle Spacings

Fig. 11

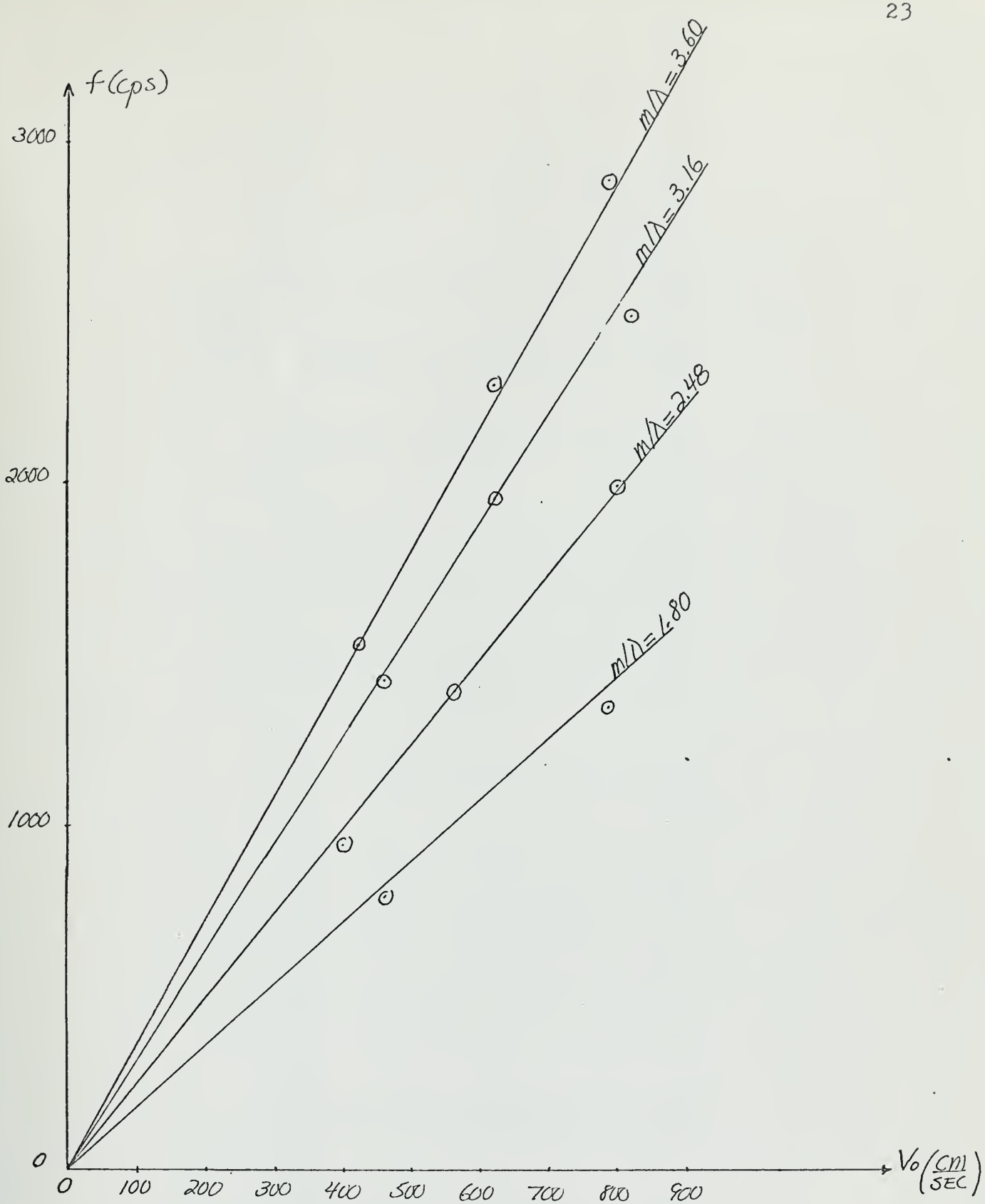

Graph of Frequency Based on 0.1 sec Count
vs
Speed of Flow as Determined by Pitot Tube

Fig. 12

Appendix 1

DATA

#	Δh	m/λ	V_o	0.1 sec count (cycles)			V_1	1.0 sec count (cycles)			V_2	Photograph count (cps) / V_3		$\frac{V_1}{V_o}$	$\frac{V_2}{V_o}$	$\frac{V_3}{V_o}$
	(cm)	(lines/cm)	(cm/sec)	high	low	avg	(cm/sec)	high	low	avg	(cm/sec)		(cm/sec)			
1	8.0	1.80	460	81	77	79.7	443	797	777	787	438	775	430	0.96	0.95	0.94
2	14.0	1.80	605	--	--	--	--	1064	1036	1050	583	1035	575	--	0.96	0.95
3	23.1	1.80	785	136	132	134.2	745	1349	1332	1342	745	1370	760	0.95	0.95	0.97
4	6.0	2.48	400	97	93	94.9	384	962	935	951	385	925	372	0.96	0.96	0.93
5	11.7	2.48	560	142	137	139.8	565	1409	1389	1399	565	1400	565	1.02	1.02	1.02
6	24.4	2.48	800	203	197	199.9	806	2009	1904	1999	806	1980	800	1.01	1.01	1.00
7	7.9	3.16	460	146	139	142.3	450	1424	1403	1412	448	1400	443	0.98	0.98	0.97
8	14.1	3.16	620	198	192	194.9	620	1967	1948	1955	621	1935	610	1.00	1.00	0.99
9	24.6	3.16	820	251	245	248.7	790	2472	2453	2465	783	2520	795	0.97	0.96	0.97
10	6.9	3.60	425	157	147	152.7	425	1544	1501	1521	423	1530	425	1.00	1.00	1.00
11	14.1	3.60	620	230	227	228.6	637	2287	2264	2280	635	2340	650	1.04	1.04	1.07
12	23.4	3.60	785	294	285	288.7	803	2911	2882	2899	807	2920	811	1.02	1.03	1.03

Appendix 2

Estimation of B_o for a Thin Lens

Let f = focal length of the lens

r = radius of the lens

m = magnification = Z_o/ξ_o

r_1 = radius of circle of confusion in the object plane

r_2 = radius of circle of confusion in the image plane

Referring to figure 1, if we let ξ be the half depth of field for a circle of confusion of diameter $2r_1$, ξ and r_1 are related as follows (5).

$$\xi = (2r_1)\ \frac{f}{2r}\ \frac{m+1}{m}$$

and $$r_1 = \frac{r\xi m}{f(m+1)}$$

Since $r_2 = mr_1 = \frac{m^2 r}{f(m+1)}$, the area of the circle of confusion in the image plane is $\pi c^2 \xi^2$, where $c = \frac{m^2 r}{f(m+1)}$.

To a first order approximation, the ratio of the area subtended by the lens to the surface area of the sphere of radius ξ_o is

$$\frac{\pi r^2}{4\pi \xi_o^2}\ .$$

Therefore the light intensity on the image plane due to a point source of unit intensity near the object plane is approximately

$$\frac{r^2}{4\ \xi_o^2}\ \frac{1}{\pi C^2 \xi^2}$$

Since the spread function is zero outside the circle of confusion in the image plane,

$$s(\bar{x} - m\bar{\xi}, \xi) = \frac{r^2}{4\pi\xi_o^2 c^2 \xi^2} \quad \text{for} \quad |\bar{x} - m\bar{\xi}|^2 \leq (c\xi)^2$$

$$= 0 \quad \text{for} \quad |\bar{x} - m\bar{\xi}|^2 > (c\xi)^2$$

Appendix 3

Fourier Transform Representation of the Reticle

The reticles used were transparencies (Polaroid type 146L projection film) made by photographing, on a Polaroid model 208 copystand, a grid of squares formed from 0.25 inch Dymo label tape. The resulting pattern was essentially the result of overlaying two equally spaced dark and transparent rulings at right angles to each other. We proceed to obtain the space representation and the Fourier transform of the reticle as follows.

For either of the parallel rulings, the space representation is decomposed into a Fourier series of the form,

$$f_1(u) = \frac{1}{2} + \frac{2}{\pi} \sum_{n=0}^{\infty} \frac{(-1)^n}{2n+1} \cos(2n+1)\frac{2\pi u}{d}$$

where u is measured along the direction perpendicular to the rulings, and d is the combined width of a dark and a transparent ruling.

This representation assigns a value of 1 to the transparent ruling and 0 to the dark ruling. Furthermore, since the rulings are not infinite in number, we multiply by a rectangle function $f_2(u) = \begin{matrix} 1 & u < \frac{1}{2} \\ 0 & u > \frac{1}{2} \end{matrix}$

If we now assume that there are integer N pairs of dark and transparent fulings, we obtain

$$f(x) = f_1(x) f_2(x/Nd)$$

$$f(y) = f_1(y) f_2(y/Nd)$$

and

$$f(x,y) = f_1(x) f_1(y) f_2(x/Nd) f_2(y/Nd)$$

The Fourier transform is given by

$$F(f_x, f_y) = \iint_{-\infty}^{\infty} f(\alpha,\beta) \exp[-i(2\pi f_x \alpha + 2\pi f_y \beta)]\, d\alpha\, d\beta$$

Since $f(\alpha,\beta)$ is a product of independent functions of α and β, we find that $F(f_x, f_y) = G(f_x)\, G(f_y)$

Now $G(f_x) = \int_{-\infty}^{\infty} f_1(\alpha) f_2(\alpha/Nd) \exp(-i 2\pi f_x \alpha)\, d\alpha$,

and, invoking the rule for transforms of products, we have

$$G(f_x) = F_1(f_x) * F_2(f_x).$$

$F_1(f_x)$ is a series of impulses at $f_x = 0$ and $\frac{2n+1}{d}$, $n = 0,1,2....$

The magnitude of these impulses are exactly the magnitude of the Fourier coefficients of the series decomposition of f_1.

$F_2(f_x)$ transforms into sin u/u form; in this case, $\frac{\sin Nd\pi f_x}{\pi f_x}$.

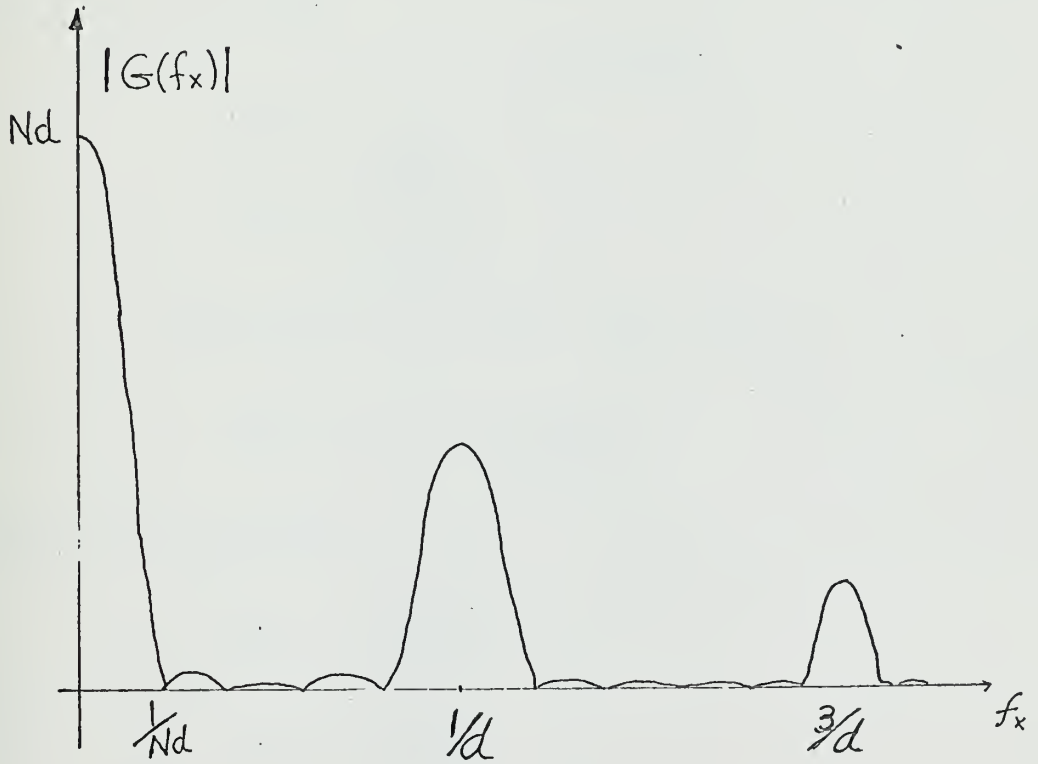

Fig 13

Appendix 4

Effect on Magnification from Transit
Through different Media

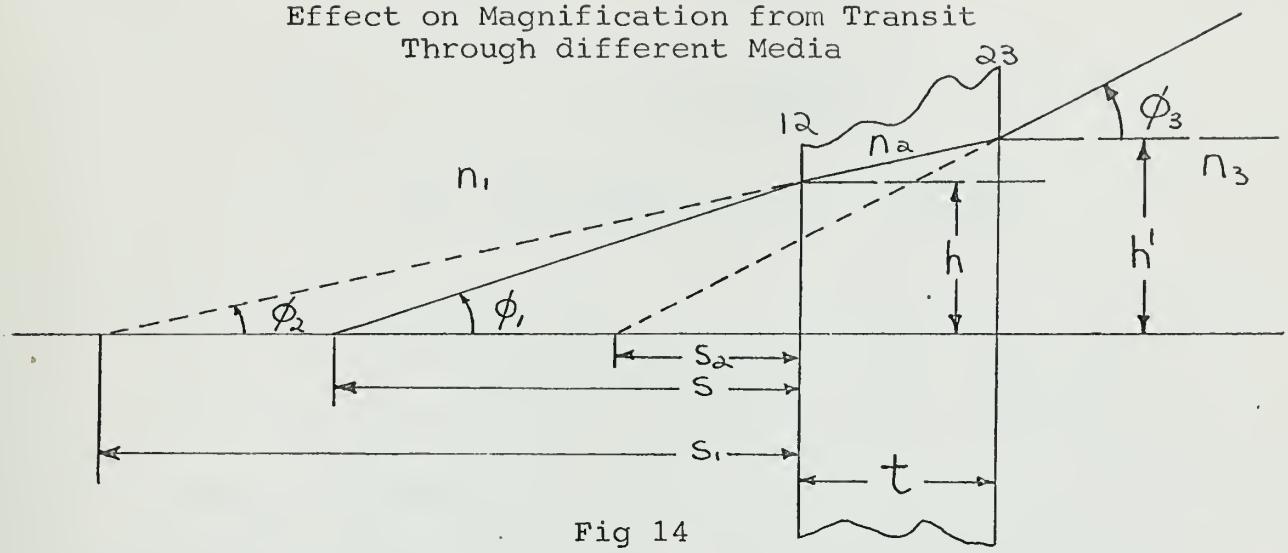

Fig 14

Let s = actual object distance

s_1 = apparent object distance due to 12 interface

s_2 = apparent object distance due to 12 and 23 interface

At the 12 interface,

$$n_1 \sin \phi_1 = n_2 \sin \phi_2$$

but $$\frac{\sin \phi_1}{\cos \phi_1} = \frac{h}{s}$$

and $$\frac{\sin \phi_2}{\cos \phi_2} = \frac{h}{s_1}$$

therefore $$n_1 \frac{h}{s} \cos \phi_1 = n_2 \frac{h}{s_1} \cos \phi_2$$

and $$s_1 = s \frac{\cos \phi_2}{\cos \phi_1} \frac{n_2}{n_1}$$

At the 23 interface,

$$n_2 \sin \phi_2 = n_3 \sin \phi_3$$

but $$\frac{\sin \phi_2}{\cos \phi_2} = \frac{h'}{s_1 + t}$$

and $$\frac{\sin \phi_3}{\cos \phi_3} = \frac{h'}{s_2 + t}$$

therefore $$n_2 \frac{h'}{s_1+t} \cos \phi_2 = n_3 \frac{h'}{s_2+t} \cos \phi_3$$

and $$s_2+t = (s_1+t) \frac{n_3}{n_2} \frac{\cos \phi_3}{\cos \phi_2}$$

or $$s_2 = s_1 \frac{n_3 \cos \phi_3}{n_2 \cos \phi_2} - t \left(1 - \frac{n_3 \cos \phi_3}{n_2 \cos \phi_2}\right)$$

Finally, letting $\Delta s = s - s_2$

$$s = s\left(1 - \frac{n_3}{n_1} \frac{\cos \phi_3}{\cos \phi_1}\right) + t\left(1 - \frac{\cos \phi_3}{\cos \phi_2} \frac{n_3}{n_2}\right)$$

For a constant object distance s, we wish to maintain Δs independent of angular variations. Therefore, we use only the paraxial rays, in which case $\cos \phi_1 = \cos \phi_2 = \cos \phi_3 \backsimeq 1$, so that

$$\Delta s = s\left(1 - \frac{n_3}{n_1}\right) + t\left(1 - \frac{n_3}{n_2}\right)$$

If we scan 2 inches of object space located in the tunnel centerline (s = 10 inches), for $n_1 \backsimeq 1.33$, $n_2 \backsimeq 1.5$, $n_3 = 1$

$$\sin \phi_1 = 0.100$$

$$\cos \phi_1 = 0.995$$

$$\sin \phi_2 = \left(\frac{1.33}{1.50}\right) 0.1 = 0.089$$

$$\cos \phi_2 = 0.996$$

$$\sin \phi_3 = \left(\frac{1.33}{1.0}\right) 0.1 = 0.133$$

$$\cos \phi_3 = 0.991$$

and $$\frac{\cos \phi_3}{\cos \phi_1} \backsimeq \frac{\cos \phi_3}{\cos \phi_2} \backsimeq 1$$

Appendix 5

931A

Multiplier Phototube

9-STAGE, SIDE-ON TYPE **S-4 RESPONSE**

For General Use in Applications Having Low Light Levels Such as Light-Operated Relays, X-Ray Exposure Control, and Facsimile Transmission

General:

Spectral Response	S-4
Wavelength of Maximum Response	4000 ± 500 angstroms
Cathode, Opaque	Cesium-Antimony
Minimum projected length[a]	15/16"
Minimum projected width[a]	5/16"
Window	Lime Glass[b]
Dynode Material	Cesium-Antimony
Direct Interelectrode Capacitances (Approx.):	
Anode to dynode No.9	4.4 pf
Anode to all other electrodes	6.0 pf
Maximum Overall Length	3-11/16"
Maximum Seated Length	3-1/8"
Length from Base Seat to Center of Useful Cathode Area	1-15/16" ± 3/32"
Maximum Diameter	1-5/16"
Operating Position	Any
Weight (Approx.)	1.6 oz
Bulb	T9
Socket	Amphenol[c] No. 78S11T, or equivalent
Magnetic Shield	Perfection Mica Co.[d], No.P-101-1, or equivalent
Base	Small-Shell Submagnal 11-Pin, (JEDEC Group 2, No.B11-88), Non-hygroscopic
Basing Designation for BOTTOM VIEW	11K

Pin 1 - Dynode No.1
Pin 2 - Dynode No.2
Pin 3 - Dynode No.3
Pin 4 - Dynode No.4
Pin 5 - Dynode No.5
Pin 6 - Dynode No.6
Pin 7 - Dynode No.7
Pin 8 - Dynode No.8
Pin 9 - Dynode No.9
Pin 10 - Anode
Pin 11 - Photocathode

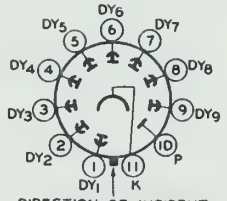

Maximum Ratings, *Absolute-Maximum Values:*

Supply Voltage Between Anode and Cathode (DC or Peak AC)	1250 max.	volts
Supply Voltage Between Dynode No.9 and Anode (DC or Peak AC)	250 max.	volts
Supply Voltage Between Consecutive Dynodes (DC or Peak AC)	250 max.	volts

← Indicates a change.

RADIO CORPORATION OF AMERICA
Electronic Components and Devices
Harrison, N. J.
DATA I
10-63

931A

Multiplier Phototube

9-STAGE, SIDE-ON TYPE **S-4 RESPONSE**

For General Use in Applications Having Low Light Levels Such as Light-Operated Relays, X-Ray Exposure Control, and Facsimile Transmission

General:

Spectral Response	S-4
Wavelength of Maximum Response	4000 ± 500 angstroms
Cathode, Opaque	Cesium-Antimony
Minimum projected length[a]	15/16"
Minimum projected width[a]	5/16"
Window	Lime Glass[b]
Dynode Material	Cesium-Antimony
Direct Interelectrode Capacitances (Approx.):	
Anode to dynode No.9	4.4 pf
Anode to all other electrodes	6.0 pf
Maximum Overall Length	3-11/16"
Maximum Seated Length	3-1/8"
Length from Base Seat to Center of Useful Cathode Area	1-15/16" ± 3/32"
Maximum Diameter	1-5/16"
Operating Position	Any
Weight (Approx.)	1.6 oz
Bulb	T-9
Socket	Amphenol[c] No. 78S11T, or equivalent
Magnetic Shield	Perfection Mica Co.[d], No. P-101-4, or equivalent
Base	Small-Shell Submagnal 11-Pin, (JEDEC Group 2, No. B11-88), Non-hygroscopic
Basing Designation for BOTTOM VIEW	11K

Pin 1 – Dynode No. 1
Pin 2 – Dynode No. 2
Pin 3 – Dynode No. 3
Pin 4 – Dynode No. 4
Pin 5 – Dynode No. 5
Pin 6 – Dynode No. 6
Pin 7 – Dynode No. 7
Pin 8 – Dynode No. 8
Pin 9 – Dynode No. 9
Pin 10 – Anode
Pin 11 – Photocathode

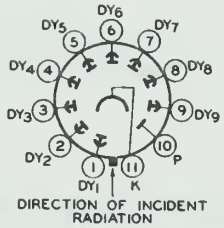

Maximum Ratings, *Absolute-Maximum Values:*

Supply Voltage Between Anode and Cathode (DC or Peak AC)	1250 max.	volts
Supply Voltage Between Dynode No.9 and Anode (DC or Peak AC)	250 max.	volts
Supply Voltage Between Consecutive Dynodes (DC or Peak AC)	250 max.	volts

← Indicates a change.

[h] At a tube temperature of 25° C. Dark current may be reduced by use of a refrigerant.

[j] For maximum signal to noise ratio, operation with a supply voltage (E) below 1000 volts is recommended.

[k] Under the following conditions: Supply voltage (E) as shown, 25° C tube temperature, external shield connected to cathode, bandwidth 1 cycle per second, tungsten light source at a color temperature of 2870° K interrupted at a low audio frequency to produce incident radiation pulses alternating between zero and the value stated. The "on" period of the pulse is equal to the "off" period.

SPECTRAL-SENSITIVITY CHARACTERISTIC
OF PHOTOSENSITIVE DEVICE HAVING S-4 RESPONSE
is shown at the front of this Section

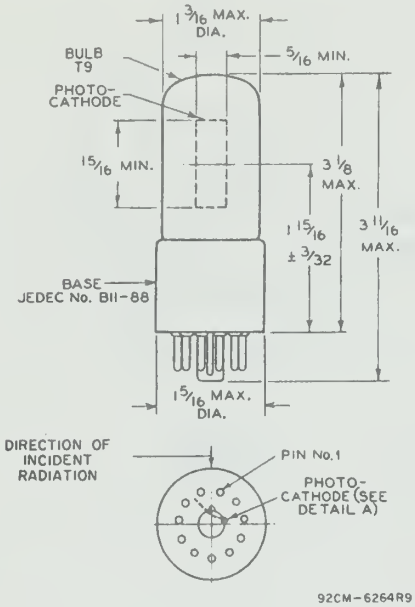

92CM-6264R9

DIMENSIONS IN INCHES

CENTER LINE OF BULB WILL NOT DEVIATE MORE THAN 2° IN ANY DIRECTION FROM THE PERPENDICULAR ERECTED AT CENTER OF BOTTOM OF BASE.

931A

DETAIL A

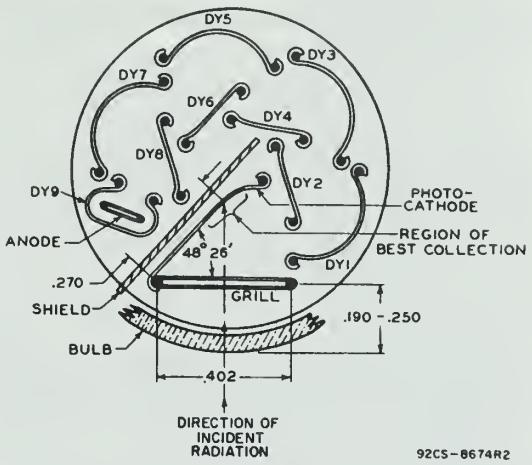

DIMENSIONS IN INCHES

931A

TYPICAL ANODE CHARACTERISTICS

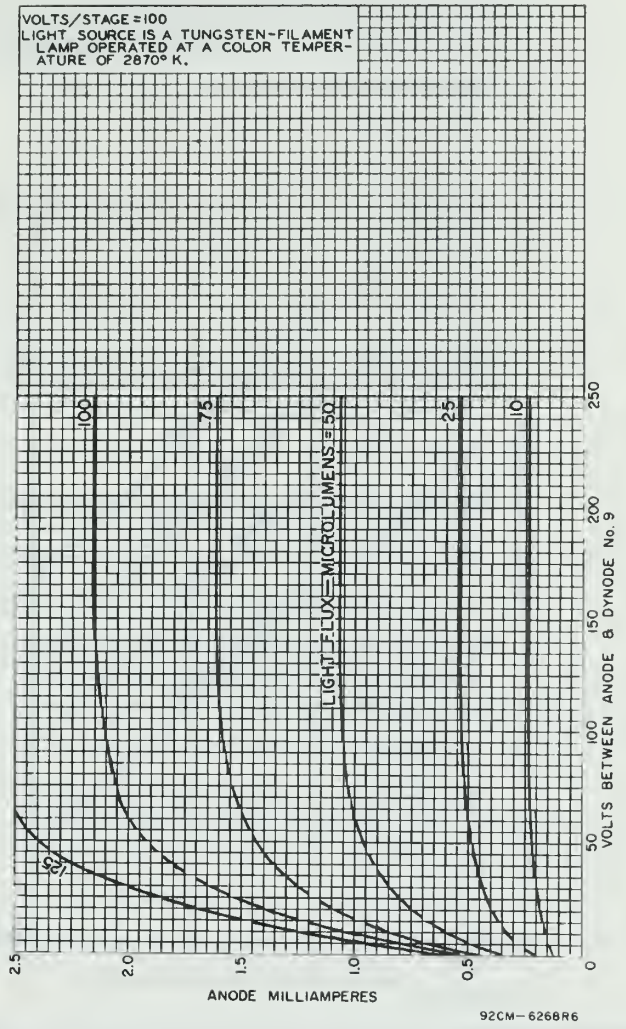

931A

SENSITIVITY AND CURRENT AMPLIFICATION CHARACTERISTICS

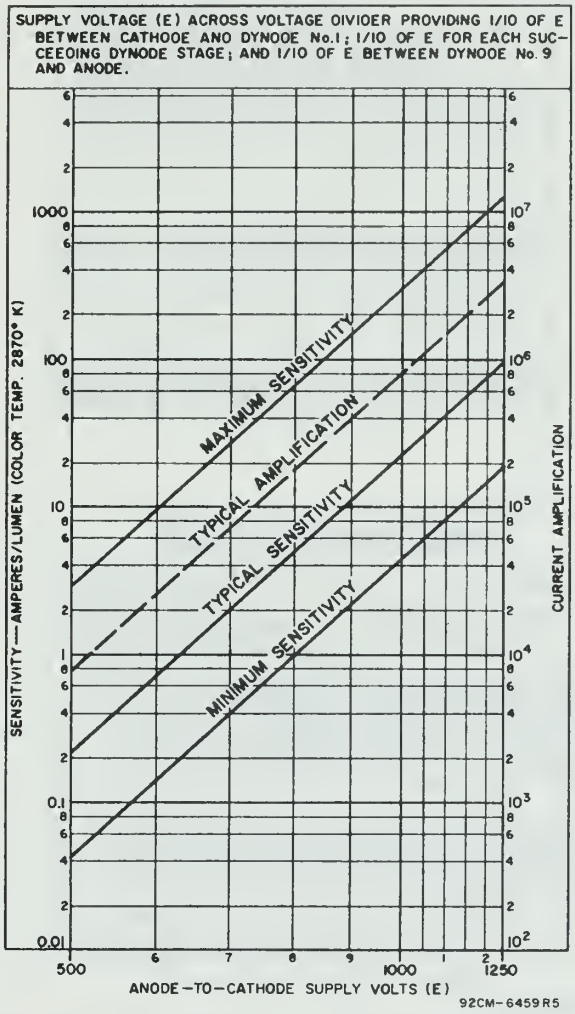

RADIO CORPORATION OF AMERICA
Electronic Components and Devices Harrison, N. J.

931A

EQUIVALENT-NOISE-INPUT CHARACTERISTIC

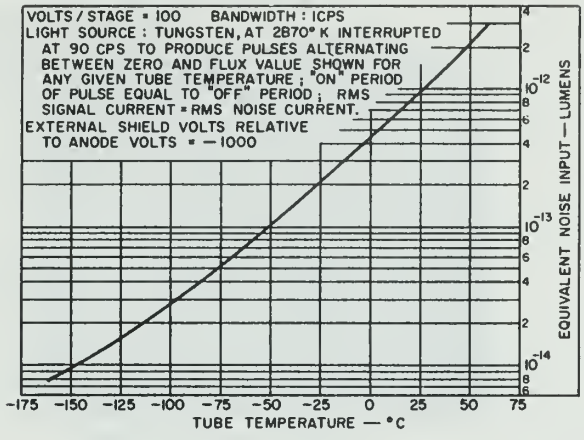

92CS-7505R2

TYPICAL EFFECT OF MAGNETIC FIELD ON ANODE CURRENT

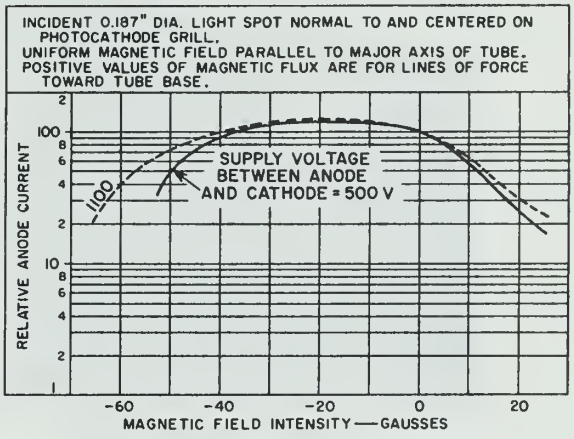

92CS-7664R2

931A

PHOTOCATHODE SENSITIVITY VARIATION ALONG ITS LENGTH

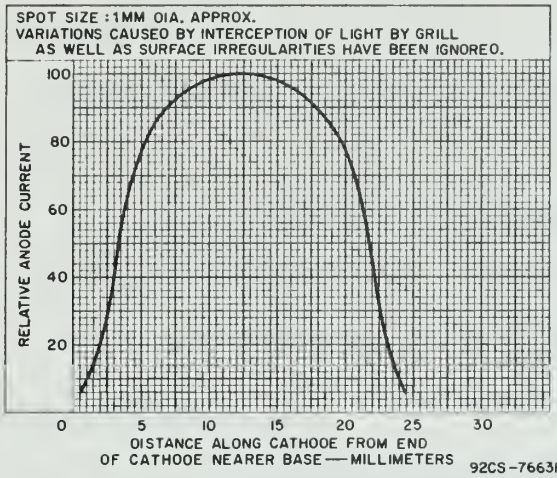

PHOTOCATHODE SENSITIVITY VARIATION ACROSS ITS PROJECTED WIDTH IN PLANE OF GRILL

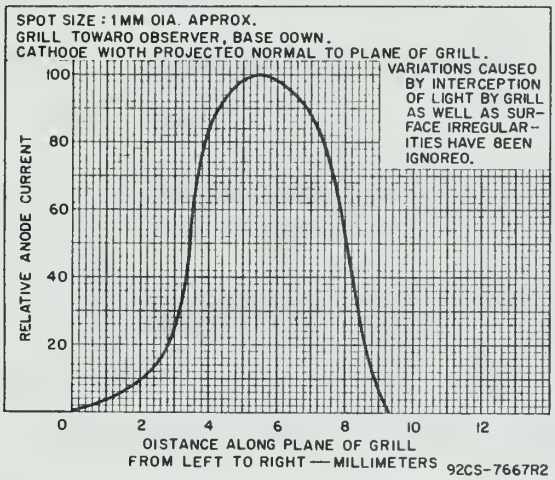

RADIO CORPORATION OF AMERICA
Electronic Components and Devices Harrison, N. J.

Bibliography

(1) Block, M.J. and Milgram, J.H., "Optical Detection of Local Fluid-Flow Velocities by Filtering in Space and Time", Journal of the Optical Society of America, 57, 5, 1967 PP 604-609

(2) Bracewell, R.M., The Fourier Transform and Its Applications, McGraw-Hill Book Company, Inc., 1965

(3) Daugherty, R.L. and Franzini, J.B., Fluid Mechanics with Engineering Applications, McGraw-Hill Book Company, Inc., 1965

(4) Jenkins and White, Fundamentals of Optics, McGraw-Hill Book Company, Inc., 1957

(5) Kingslake, R., Lenses in Photography, A.S. Barnes and Company, Inc., 1963

(6) O'Neill, E.L., Introduction to Statistical Optics, Addison-Wesley, 1963

(7) Papoulis, A., The Fourier Integral and Its Applications, McGraw-Hill Book Company, Inc., 1962

(8) Ramo, J., Whinnery, J.R. and Van Duzer, T., Fields and Waves in Communications Electronics, John Wiley and Sons, Inc., 1965

(9) Shames, I.H., Mechanics of Fluids, McGraw-Hill Book Company, Inc., 1962

(10) Stewart, W.A., "System for Measuring Instantaneous Fluid Velocity without Interfering With the Flow", M.I.T. ScD Thesis (M.E.) 1959